Gas production behaviour of gas hydrate–bearing clayey-sand during depressurization: novel in-flight centrifuge modelling

Sina Baghbanrezvan[1*], and *Charles wang wai* Ng[2]

[1]Geotechnical Centrifuge Facility, Hong Kong University of Science and Technology, Clear Water Bay, Kowloon, Hong Kong SAR
[2]Department of Civil and Environmental Engineering, Hong Kong University of Science and Technology, Clear Water Bay, Kowloon, Hong Kong SAR

Abstract. Gas hydrate-bearing sediments (GHBS) are vastly distributed around the globe. While gas production attempts are made through GHBS, long-term production remains a challenge due to complex inter-related mechanisms involved. Better understating of long-term responses requires sound physical modelling conducted under controlled conditions. A novel centrifuge energy harvesting chamber (CEHC) at the HKUST centrifuge facility is used in this study. This is the first chamber that can operate at elevated gravities with the capability of sustaining the thermodynamically favourable conditions for gas hydrate formation, sustaining a continuous inflow of high-pressure water at the boundaries during dissociation, and an in-flight control of wellbore pressure and surcharge loading. Centrifuge modelling can recreate the in-situ stress gradient in a relatively small model and expedite conduction and convection processes involved during dissociation. Consequently, long-term in-situ mechanisms can be evaluated with a small model and short time. A test was conducted at 40g to evaluate the temperature-pressure response as well as gas production behaviour of hydrate-bearing clayey-sand during depressurization. The results suggests that the gas flow rate is governed by the initial available latent heat as well as the conduction and convection heat through the surrounding sediments. However, as the depressurization progresses, the gas production rate is governed by the competing effects of hydrate dissociation and re-formation which both evolves the permeability of the sediment. Details of the experiment and test results are reported in this paper.

1 Introduction

Gas hydrates are solid ice-like crystals consisting of a host gas molecule surrounded by water molecules. Due to their abundance, methane hydrate-bearing sediments (MHBS) have been considered as a potential source of natural gas for future. A distinct characteristic of methane hydrates is that they are only stable under thermodynamically favourable conditions of relatively high pore pressures and low temperatures.

The presence of methane hydrate in soil pores alters the hydro-mechanical behaviour of the sediment bearing it. Since methane hydrates are stable at specific pressures and temperatures, the key to the extraction of methane gas from hydrates lies behind driving hydrates out of their thermodynamically stable conditions (i.e. dissociation).

The measurements obtained from trial field gas production tests are useful since they allow for an actual performance to be assessed. However, these studies are time-consuming and costly due to the process of drilling into the sediments below the seabed. In addition, the interpretation of data obtained from trial field gas production tests is challenging due to the high natural variability in the degree of hydrate saturation in natural deposits. Although numerical tools are important to further our understanding of GHBS response during depressurization, the obtained results and observed mechanisms are not thoroughly validated due to the lack of experimental data

Physical model tests at 1g (i.e., the Earth's gravity g = 9.81 m/s2) are useful for studying the production flow rates and evaluating the influencing factors for an efficient gas extraction method. However, 1g physical tests are deemed to be not suitable for studying the interaction between a structure (e.g., wellbore casing) and the surrounding sediment due to the lack of scaling and mimicking the correct stress state of the soil. Hence, centrifuge model tests have yet to emerge for studying the complex behaviour of soil during gas extraction from MHBS and providing high-quality data for the calibration of numerical models. This can provide a better understanding of the interaction between MHBS and the wellbores before advancing toward a feasible gas extraction from these sediments in the future. Therefore, more centrifuge model tests in controlled boundary conditions and known variables are required.

In this study, a novel centrifuge test is carried out using the newly developed CEHC inflight. Depressurization-induced hydrate dissociation is simulated through a vertical wellbore in GHBS. Evolutions of temperature and pore pressure during gas

* Corresponding author: sina@ust.hk

hydrate formation as well as the depressurization-induced dissociation are presented. New insights into the gas production behaviour of gas hydrate–bearing clayey-sand and reservoir response are provided.

2 Model setup and instrumentation

A novel centrifuge energy harvesting chamber (CEHC) at the HKUST centrifuge facility is used in this study [1]. This is the first chamber that can operate at elevated gravities with the capability of sustaining the thermodynamically favourable conditions for gas hydrate formation, sustaining a continuous inflow of high-pressure water at the boundaries during dissociation, and an in-flight control of wellbore pressure and surcharge loading. Figure 1 shows the model geometry and instrumentation in the test on the hydrate-bearing sand-clay mixture. The excess gas method was used to form CO_2 hydrate formation in a Toyoura sand-clay mixture with 15% of clay content by weight. The gravimetric water content of 12.3% was added to the sand-clay mixture which was compacted in 7 layers (each 10 cm) inside the chamber to the target void ratio of 0.81 (Dr = 45%). After each layer was compacted, thermocouples (TC) were positioned at designated locations. Details of the instrumentation are shown in Figure 1, where the geometry is shown in the model scale. Out of safety reasons, carbon dioxide (CO_2) instead of methane was used as the hydrate-forming gas in this study. After preparing the column, the chamber was thermally insulated with polyurethane foam and was pressurized with CO_2 gas. The CO_2 pressure was increased to about 3.1 MPa and kept constant during the whole hydrate formation stage. The temperature was also decreased to initiate hydrate formation. The estimated degree of hydrate saturation in this test was approximately 45−52% considering the possible hydrate dissolution and reformation.

The relevant scaling laws for the centrifuge test in this study are summurised in Ng et al[1]. The depressurization test was conducted at 40 times the gravity of the Earth (40g) in the centrifuge. In the prototype, the model represents a 28 m thick GHBS below the sea surface. Hence, the objective of this study is to simulate a gas hydrate-bearing sand-clay mixture at shallow depths. The total duration of the test in the model scale was 8.7 hours, corresponding to 580 days in the prototype. Mass and heat flows occur 1600 times faster in the model compared to the prototype since the conduction and convection are N^2 times faster in the centrifuge model than the prototype The size and the material of the miniature wellbore casing in this test are selected to fulfill the scaling of the axial stiffness (i.e., $1/N^2$) and dimensions (i.e., $1/N$) of the typical prototype casing. An aluminum vertical wellbore casing with Young's modulus of 70 GPa, which has a perforated interval of 4 m in prototype as the gas production region, was used in this study. The perforated region is highlighted in Figure 1. Its diameter and wall thickness were 10 mm and 0.5 mm, respectively. This would represent in the prototype a typical 9-5/8-inch casing used in the second production test in the Nankai Trough [2]. To prevent sand production during depressurization, the perforated interval was covered by geotextile with an apparent opening size (AOS) of 75μm to avoid sand from getting into the casing. To monitor pore pressure, three pressure transducers were installed at the wellbore, top, and side boundaries.

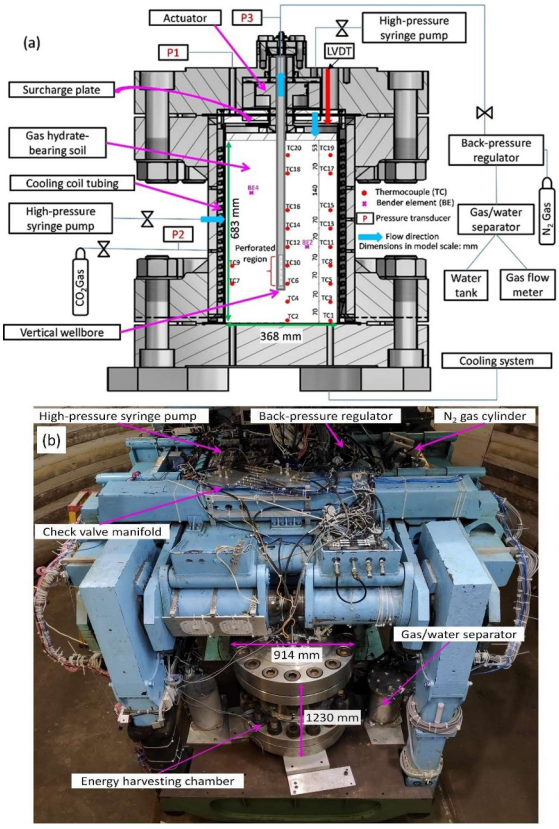

Fig. 1. Centrifuge energy harvesting chamber (CEHC): a) Schematic diagram of the chamber setup and instrumentation; b) chamber setup and all the components on the centrifuge platform

2.1 Temperature- pressure response during gas hydrate formation

Figure 2 shows the temperature response of 4 selected thermocouples at different locations inside the chamber during the hydrate formation process. The temperature of the precooled chamber was increased initially during the gas injection due to the ideal gas law. The temperature was then gradually decreased by the cooling unit and brought inside the stability region of CO_2 hydrate and kept within the temperature range of 0-4 °C until the hydrate formation was ceased.

Temperature spikes due to an exothermal reaction of hydrate formation [3] were observed. Most of the temperature spikes were observed during the first four days of the hydrate formation process, indicating that most of the hydrate was formed during this period. Hydrate formation in small pores is influenced by the capillary effect, which shifts the thermodynamic phase boundary to lower temperatures (or higher pressures). This phenomenon is called melting point depression (or dissociation temperature depression), often referred to as the Gibbs−Thomson effect [4].

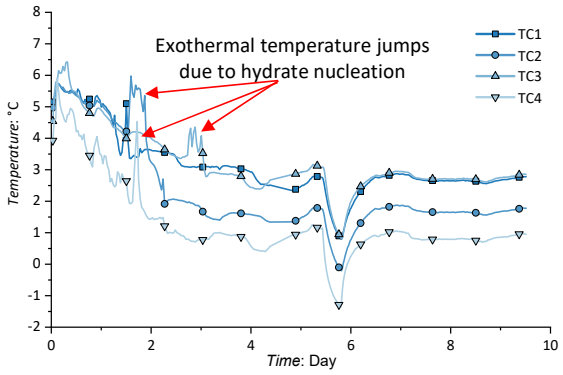

Fig. 2. Temperature response during CO_2 hydrate formation

Since the sand-clay mixture in this test consists of clay with smaller pores than sand, the temperature was further reduced by cooling the chamber between days 5 and 6 to initiate the transformation of any remaining water inside the smaller pores into hydrate. However, no apparent temperature spike was observed, indicating that most of the water was transferred into the hydrate. The temperature was then increased above zero before saturation of the chamber with water while keeping the temperature-pressure state inside the stability region.

By taking the average value of the pressure at the two boundaries, the temperature-pressure response during CO_2 hydrate formation together with the phase boundary of CO_2 hydrate [3] in the temperature and pressure plane is plotted in Figure 3. All the measurements are located inside the stable region for CO_2 hydrate during the whole process of hydrate formation.

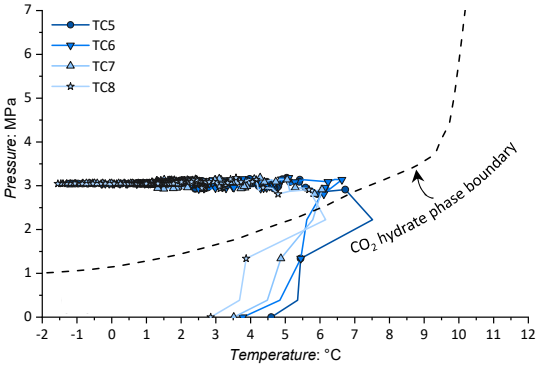

Fig. 3. Temperature-pressure response during CO2 hydrate formation phase boundary of CO2 hydrate in temperature and pressure plane is plotted from Sloan and Koh (2008)

3 Gas hydrate dissociation

Following the hydrate formation, the pore water pressure was adjusted to about 6.5 MPa (about 650 m of water pressure in the prototype) and the chamber was spun up to 40g in the centrifuge. The wellbore pressure was decreased to induce hydrate dissociation through the perforated area of the wellbore casing while keeping the boundary pressures inside the stability region through a constant influx of high-pressure water. All the dimensions are presented in porotype unless otherwise stated.

3.1 Wellbore and boundaries pore pressures

Figure 4 shows the testing sequence and the pressure of the wellbore and the boundaries throughout the test. During the spin-up of the centrifuge, the pressure increased due to the elevated gravity of the centrifuge. The pressure increase was larger at the permeable side boundary, while this increase at the wellbore casing perforation was smaller due to the low permeability of the hydrate-bearing sand-clay mixture. After reaching an equilibrium at about 104 days after the spin-up, the depressurization was induced by decreasing the wellbore's pressure to approximately 0.5 MPa while keeping the continuous influx of water through the boundaries.

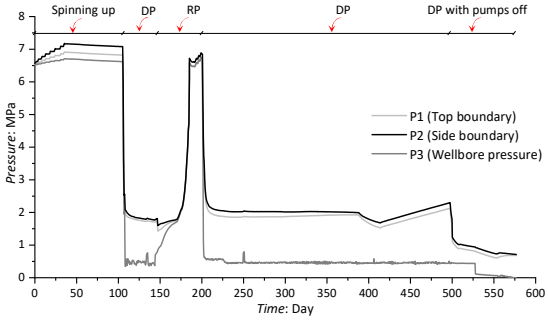

Fig. 4. The centrifuge testing sequence and the chamber performance during simulating the gas hydrate dissociation in the centrifuge (at 40g); DP and RP denote depressurization and re-pressurization stages, respectively

This resulted in a localized depressurization and an increase in the effective stresses in the vicinity of the wellbore casing perforations, which expanded over time as the depressurization front evolved. Since the re-pressurization stage of the chamber in the previous test on hydrate-bearing sand [1] had no significant effect on the wellbore's overall behaviour, depressurization was planned to be carried out in one stage in the current test. However, due to some difficulties in controlling the pumps and the back-pressure regulator, a re-pressurization stage was carried out at 143 days (after 40 days of depressurization). Due to the presence of the compressible gas and the hydrate-bearing sand-clay mixture's low permeability compared to the hydrate-bearing sand [1], the re-pressurization stage took longer to reach the pressure of 6.5 MPa. After reaching the target pressure of 6.5 MPa, another stage of depressurization was carried out from 200 to 500 days (a total of 300 days of depressurization in the prototype). The depressurization was continued with the pumps off at the end of the experiment to evaluate the total produced gas. This stage is similar to the depressurization tests conducted in the literature where the whole chamber is depressurized rather than the local depressurization in the wellbore's vicinity.

3.2 Temperature-pressure response and hydrate reformation

Figure 5 shows the temperature measurements during the whole experiment at different locations inside the chamber. The measurements of 16 thermocouples are

presented since four of the thermocouples (TC17, TC18, TC19 and TC20) were not responding during the test. With the start of depressurization on the 103rd day, the temperature at TC6, TC10 (Fig. 5(b)) located in the vicinity of the perforated region decreased significantly, which implies the initiation of hydrate dissociation in this region. The decrease in the temperature continued until the 143rd day, which was the end of the first depressurization stage. The temperature decrease was also observed at TC2, TC4, TC7, and TC9 but with a lower decrease rate implying a smaller amount of hydrate dissociation in those regions further from the wellbore perforations. Interestingly, a temperature jump was observed at TC12 (Fig 5 (c)) on about the 140th day of the test. This temperature jump implies hydrate reformation at this location due to the produced CO_2 gas and water availability. Although TC12 is relatively close to the perforated region, and it might be expected that the temperature-pressure state should be outside the stability region, the pressure build-up of the entrapped produced CO_2 gas inside the small pores of low permeability hydrate-bearing sand-clay mixture can derive the pressure state inside the stability region. Consequently, a local hydrate reformation can be induced. A more obvious hydrate reformation is observed in the second stage of depressurization, which will be discussed later in this section. Such behaviour was not observed in hydrate-bearing sand [1], probably due to a higher permeability of the sediment without clay content. It should be pointed out that the continuous increase in the temperature due to the influx of higher-temperature water into the chamber (as was observed by Ng et al [1]) is mostly eliminated in the current test with better insulation of the water tank and the pumps. Hence, the temperature increase in this test is solely due to the exothermic reaction of hydrate reformation. No obvious change in temperature was observed during the re-pressurization stage.

With the start of the second stage of depressurization on the 200th day, another temperature drop was induced in the vicinity of the wellbore. However, the temperature drop ceased quickly, which was followed by a temperature increase at TC4 (Fig.5 (a)), TC6, TC7, TC9, TC10 (Fig.5 (b)) and TC5, TC12 (Fig.5 (c)) until about 380th day. During this period of depressurization, the two competing processes of hydrate dissociation and reformation took place. The hydrate dissociation was triggered by the decrease in the pressure inducing the pressure gradient from the boundaries to the wellbore perforations, while hydrate reformation was induced due to the gas pressure build-up in confined smaller pores with lower permeability sediment. The gas hydrates in these locations were deemed unstable with depressurization, while the stability conditions were often quickly restored by endothermic hydrate dissociation and pressure build-up. During this period, the hydrate reformation was more dominant, which hindered continuous gas production, as will be shown later in this paper.

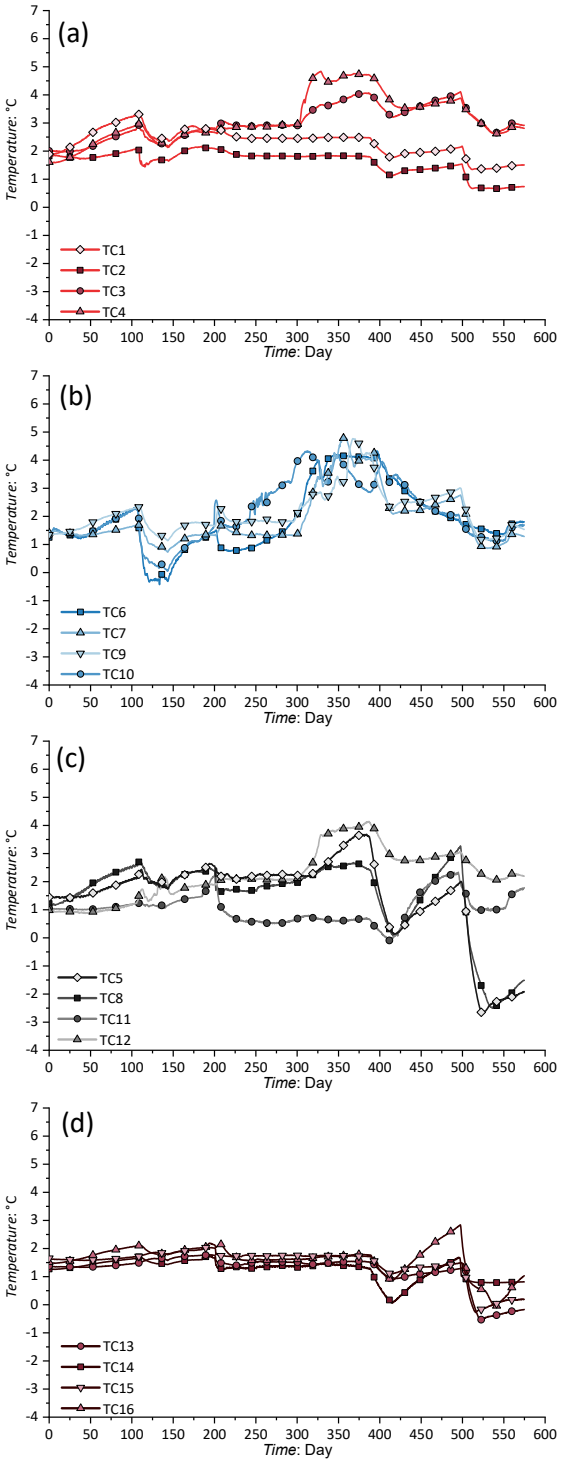

Fig. 5. The temperature response at different locations in the reservoir during the centrifuge test (a-d)

With the progression of depressurization and the continuous water supply from the boundaries, a temperature drop was observed in all the thermocouples between 380th and 400th day. The temperature drops at TC5, TC8, TC11, and TC12 were more significant, indicating a more pronounced hydrate dissociation at those locations. This temperature drop implies that the hydrate dissociation was more dominant during this period. Another temperature rise was induced at TC5,

TC8, TC11, TC15, and TC16 due to the build-up of dissociated gas pressure and hydrate reformation. This behaviour was not observed in the experiment in hydrate-bearing sand [1] due to the higher permeability of the sand than the sand-clay mixture. The hydrate reformation continued towards the end of the test at 500 days when the pumps were turned off, and the whole chamber was depressurized to induce hydrate dissociation in the remaining hydrate in the soil. At this stage, the extent of temperature drop can indicate where the hydrates were still available until 500 days. A more pronounced temperature drop clearly indicates a higher hydrate saturation at the locations far from the wellbore perforations.

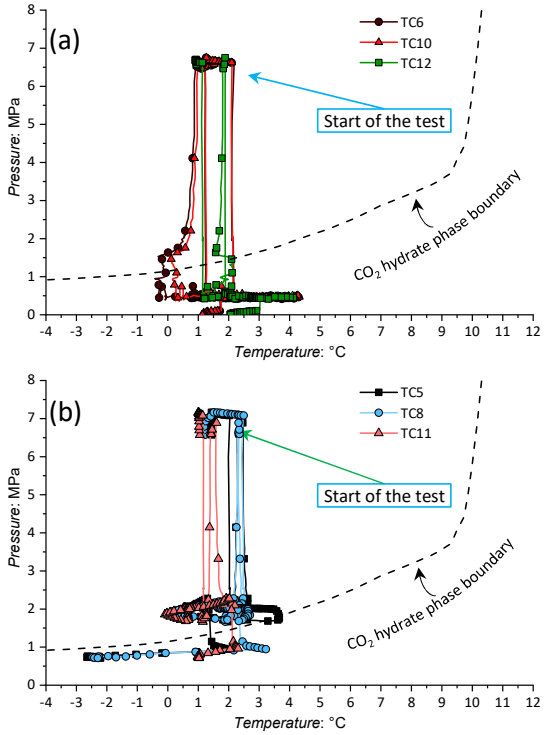

Fig. 6. Temperature-pressure response during gas hydrate dissociation in the centrifuge (at 40g): a) in the vicinity of casing perforations; b) side boundary

The temperature-pressure response of the three thermocouples near the wellbore perforation as well as three thermocouples near the side boundary are shown in Figure 6 with respect to the CO_2 hydrate phase boundary. Due to the lack of pressure transducers inside the soil, it was assumed that the pressures at TC6, TC10, and TC12 were equal to the wellbore pressure while the pressures at TC5 TC8, and TC11 were equal to the pressure at the side boundary (P2). Similar to the results by Ng et al [1], the temperature-pressure state in the vicinity of the wellbore (Figure 6 (a)) was located outside the stability region during both stages of depressurization. On the other hand, the pressure-temperature state at the boundaries (Figure 6 (b)) did not reach the hydrate phase boundary during the first stage of depressurization, while the distance from the hydrate phase boundary reduced during the second stage of depressurization. This implies that the hydrate dissociation front expanded due to the permeability and pressure field evolution during the hydrate dissociation.

Lastly, the final stage of the test with the pumps off resulted in moving the temperature-pressure state at all locations outside the stability region, resulting in the dissociation of most of the available hydrate.

3.3 Gas production behaviour

Figure 7(a) shows the gas flow rate and normalised cumulative produced gas during different stages of the experiment. With the start of the first stage of depressurization on the 103rd day, the gas flow rate showed an immediate surge followed by a gradual decline with continuous depressurization until 143rd day. The observed initial gas flow surge was due to the dissociation of hydrates in the vicinity of the perforated area as shown in the schematic temperature response in Figure 5 (b). As the endothermic hydrate dissociation consumes the latent heat, the gas flow rate decreases with the duration of depressurization.

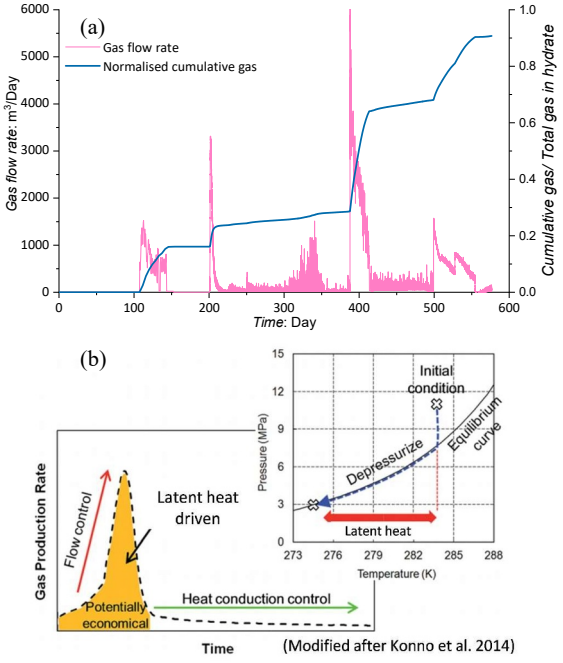

Fig. 7. Gas production behaviour: a) gas flow rate and normalised cumulative produced gas; b) schematic diagram of gas production rate evolution

In this stage, the change in the gas flow rate is governed by the conduction and convection of heat through the surrounding sediments which are within the stability region. This behaviour is similar to the schematic diagram presented in Figure 7 (b). As expected, as the re-pressurization stage initiates, the gas flow rate reached zero value. By the start of the second stage of depressurization on the 200th day, an early gas surge followed by a fast decline and a subsequent irregular pattern of peaks were observed until the 380th day. The initial fast surge was mainly the result of the flow of dissociated gas bubbles from the first stage of dissociation, which was entrapped in the sediment and could not coalesce and form a continuous gas. The presence of gas would result in an unsaturated media and affect the gas and water permeability of the reservoir.

With the progression of depressurization, the dissociation front tended to expand in the depth and radial directions. However, the hydrate reformation decreased the permeability of the sediment, entrapping more gas bubbles, which resulted in a pressure build-up in the small pores of the sediment. Consequently, the gas flow rate was governed by hydrate dissociation (increase in the permeability) and a more dominant hydrate reformation (decrease in the permeability) in this stage, as shown in Figure 5, which illustrates the temperature increase due to the exothermic hydrate reformation. The continuous hydrate reformation decreased the gas flow rate substantially until the 380th day in which subsequent gas accumulation induced local pressure build-up and fracturing in areas of high gas hydrate saturation with low permeability. This was followed by a surge in the gas flow rate on the 380th day and further expansion of the dissociation front from the wellbore perforation area, which was consistent with the temperature response in Figure 5. The gas flow rate was yet again interrupted and followed by a decline with a subsequent irregular pattern of peaks by hydrate reformation which lasted until the end of the depressurization test at about the 500th day. At the 500th day, the pumps were turned off and the whole chamber was depressurized, resulting in a surge in the gas flow rate with the dissociation of the remaining gas hydrates in the soil. Compared to the results of 1g physical model tests on hydrate-bearing sand [5,6] as well as the centrifuge model results on gas hydrate-bearing sand [1], the current experiment is the first to observe such a unique hydrate reformation which signifies the important role of the fine particles in controlling the permeability evolution during hydrate reformation and hence the gas production behaviour.

To evaluate an approximate estimate of the percentage of the dissociated hydrate with the time of depressurization, the ratio of the cumulative produced gas to the total available gas in hydrates inside the chamber is plotted against time in Figure 7 (a). At the end of the first depressurization stage, about 16% of the total available gas was produced. Given the fast surge of gas flow rate with the start of the second depressurization stage, it is expected that more than 16% of the hydrate was dissociated in the first depressurization stage. At the end of the second depressurization stage, about 69 % of the total available gas was dissociated. However, the increase in the cumulative produced gas in the second depressurization stage was not uniform, which was interrupted by a continuous gas hydrate reformation. Finally, 91% of the total available gas could be produced at the end of the experiment and before spinning down the centrifuge. The 9% of the remaining gas could be entrapped inside the sediment since as shown in Figure 5, the soil should have been frozen due to the endothermic hydrate dissociation hindering the flow pathways to the wellbore perforation.

4 Summary & conclusions

This paper presents the effects of hydrate dissociation on the gas production behaviour of gas hydrate–bearing clayey-sand and reservoir response. The results indicated that the addition of 15% clay content significantly altered the temperature-pressure response in gas hydrate-bearing sand. The temperature and pressure evolved continuously during depressurization due to the evolution of the permeability. Two competing processes of hydrate dissociation and reformation took place. The hydrate dissociation was triggered by the decrease in the pressure inducing the pressure gradient from the boundaries to the wellbore perforations, while hydrate reformation was induced due to the gas pressure build-up in confined smaller pores with low permeability sediment. The gas hydrates in these locations were deemed unstable during depressurization, while the stability conditions were often quickly restored by endothermic hydrate dissociation and pressure build-up. With the start of the first stage of depressurization, the gas flow rate reached an immediate surge following a gradual decline. As the endothermic hydrate dissociation consumed the latent heat, the gas flow rate decreased with depressurization. In this stage, the change in the gas flow rate was governed by heat conduction and convection through the surrounding sediments. However, as depressurization progressed, the gas production rate was governed by the competing effects of hydrate dissociation and reformation, which evolved the permeability of the sediment continuously.

Acknowledgments

The authors would like to acknowledge the Research Grants Council of the Hong Kong Special Administrative Region for providing us the research grants 16210420, 16207819, 16207918 and 16204817.

References

1. C. W. W. Ng, S. Baghbanrezvan, S. Y. Lau, M. Sanchez, C. Zhou. J. Geotech. Geoenviron. Engng. **148**, 3, 04021199 (2022)
2. K. Yamamoto, X. X. Wang, M. Tamaki, K. Suzuki. RSC. Adv. **9**, 45, 25987-26013 (2019)
3. E. Sloan, C. Koh. *Clathrate hydrates of natural gases*. Boca Raton, FL: CRC Press (2008)
4. T. Park, J. Y. Lee, T. H. Kwon. Energy Fuels. **32**, 4, 5321-5330 (2018)
5. Y. Konno, Y. Jin, K. Shinjou, J. Nagao. RSC. Adv. **4**, No. 93, 51666-51675 (2014)
6. K. U. Heeschen, S. Abendroth, M. Priegnitz, E. Spangenberg, J. Thaler, J. M. Schicks. Energy Fuels. **30**, 8, 6210-6219 (2016)